



# Probing topology of supramolecular complexes between cyclodextrins and alkali metals by ion mobility-mass spectrometry

Cédric Przybylski, Véronique Bonnet

## ► To cite this version:

Cédric Przybylski, Véronique Bonnet. Probing topology of supramolecular complexes between cyclodextrins and alkali metals by ion mobility-mass spectrometry. Carbohydrate Polymers, 2022, 10.1016/j.carbpol.2022.120019 . hal-03931502

**HAL Id: hal-03931502**

**<https://hal.sorbonne-universite.fr/hal-03931502>**

Submitted on 9 Jan 2023

**HAL** is a multi-disciplinary open access archive for the deposit and dissemination of scientific research documents, whether they are published or not. The documents may come from teaching and research institutions in France or abroad, or from public or private research centers.

L'archive ouverte pluridisciplinaire **HAL**, est destinée au dépôt et à la diffusion de documents scientifiques de niveau recherche, publiés ou non, émanant des établissements d'enseignement et de recherche français ou étrangers, des laboratoires publics ou privés.

1    **Probing topology of supramolecular complexes between cy-**  
2    **lodextrins and alkali metals by ion mobility-mass spectrom-**  
3    **etry**

4    Cédric Przybylski<sup>a,\*</sup> Véronique Bonnet<sup>b</sup>

5    <sup>a</sup> Sorbonne Université, CNRS, Institut Parisien de Chimie Moléculaire, IPCM, 4 Place Jussieu, 75005 Paris, France.

6    E-mail: [cedric.przybylski@sorbonne-universite.fr](mailto:cedric.przybylski@sorbonne-universite.fr)  
7

8    <sup>b</sup> Université de Picardie Jules Verne, Laboratoire de Glycochimie, des Antimicrobiens et des Agroressources, LG2A,  
9    CNRS, 33 rue Saint Leu, 80039 Amiens, France.

## ABSTRACT

In this study, the size and shape of supramolecular assemblies between cyclo-oligosaccharides and proton, ammonium or a series of alkali metals by electrospray coupled to trapped ion mobility-mass spectrometry (ESI-TIMS) have investigated. Native cyclodextrins (CD) were selected as models, and collision cross section (CCS) values were deducted for the main positive singly and doubly charged species. Experimental CCS values were in good agreement with those obtained from molecular modeling. Due to the high mobility resolving power and resolution, it was possible to highlight the presence of various conformers. Also, TIMS allowed to discriminate and estimate the content of various orientations from non-covalent nanotubes-based CD, involving secondary/secondary rim hydroxyl groups (head-to head), primary/secondary rim (head-to-tail) hydroxyl groups or primary/primary rim (tail-to-tail) hydroxyl groups interactions. Such results pave the way for a better knowledge of the topology of cyclo-oligosaccharides based supramolecular complexes, demonstrating that TIMS can be a particularly attractive molecular descriptor.

**Keywords:** Cyclo-oligosaccharides; Cyclodextrins; Supramolecular assembly; Conformers; Ion-mobility; Mass spectrometry.

## 1. INTRODUCTION

Starch is among the most abundant polysaccharides present in the plant kingdom. It is composed of numerous glucose (Glc) units predominantly linked by  $\alpha$ -(1→4) glycosidic bonds and occasionally branched by  $\alpha$ -(1→6) moderately long chains.(Tester et al., 2004)

The combined action of enzymes such as  $\alpha$ -amylase and cyclodextrin glycosyltransferase, has attracted major interest from industry due to their unique capacity to catalyse the formation of  $\alpha$ -(1→4) malto-oligosaccharides as linear (maltodextrins) or cyclic ones (cyclodextrins; CDs) all with possible branching in  $\alpha$ -(1→6).(Ao et al., 2007; French et al., 1965; Taniguchi & Honnda, 2009; Terada et al., 1997) On the basis of the number of residues, commercially available CDs are torus-shaped cyclic oligosaccharides composed of 6, 7 and 8  $\alpha$ -(1→4) linked D-glucopyranose units for  $\alpha$ -CD,  $\beta$ -CD, and  $\gamma$ -CD, respectively.(Szejtli, 1998)

CDs form a hydrophobic cavity able to encapsulate several organic molecules,(Kfoury et al., 2018; Song et al., 2009) and exhibit peripherally hydrophilic features forming intra- and inter-molecular networks thanks to hydrogen bonds.(Loftsson et al., 2005) Such particular properties is abundantly exploited to form various inclusion complexes in many industrial and research fields like food, flavours, cosmetics, drug delivery, catalyst or chiral selectors amongst other.(Davis & Brewster, 2004; Singh et al., 2002; Szejtli, 1998; Szente & Szemán, 2013)

Also, the non-bonding electron pairs of the glycosidic oxygen bridge directed towards the inside of the cavity lead to a high electron density which lends CDs some Lewis base character.(Saenger, 1980; Szejtli, 1998; Wenz, 1994) Moreover, the 6-hydroxyl group of the primary rim can constitute very good attachment sites for various metals.(S. Angelova et al.,

2017; S. E. Angelova et al., 2017; Dossmann et al., 2021; Przybylski et al., 2015) One of the central concepts of molecular recognition is the issue of “selectivity”, i.e. the preferential binding of one guest over another by the host. In this sense, one of the elusive structural characteristics when studying CD complexation is how the cavity shape changes upon complexation. Hence, the determination of effective complexation, as well as size and shape of host with and without any guest at a molecular level are mandatory conditions. In a common way, such piece of information was commonly accessed using NMR based diffusion experiments,(Schneider et al., 1998) X-ray diffraction analysis(Steiner & Koellner, 1994) and molecular modeling.(Quevedo & Zoppi, 2018)

Nonetheless, the introduction of a new technology, named ion mobility coupled to mass spectrometry (IM-MS), offers a promising complementary tool to reach aforementioned objectives. IM-MS have successfully been applied to the gas-phase ion separation of a large range of (bio)molecules based isomers such as peptides/proteins, oligonucleotides, lipids, glycans, synthetic polymers or complexes.(Ben-Nissan & Sharon, 2018; Butcher et al., 2018; Charles et al., 2020; Dodds & Baker, 2019; Gray et al., 2016; Kalenius et al., 2019; Li et al., 2020; Zheng et al., 2018) Unfortunately, its potentiality in supramolecular assemblies investigations remains still underestimated.(Kalenius et al., 2019; Polewski et al., 2021) Such discrimination based on structural differences can be characterized by determination of their collision cross section (CCS) values in a given gas. Of special interest, IM-MS has been previously applied to CDs analysis using different instrumental configurations such as matrix-assisted laser desorption or electrospray coupled to drift-tube ion mobility spectrometry (ESI-DTIMS). (Liu & Clemmer, 1997; Klein et al., 2018;Fenn & McLean, 2011; S. Lee et al., 1997)

ESI with Traveling-Wave Ion Mobility Spectrometry (ESI-TWIMS) was used to study negatively charged mono- to trimeric  $\beta$ -CD (Berland et al., 2014), or positively charged complexes like amino- $\beta$ -CD/sesamins, (Sugahara et al., 2015)  $\alpha$ - and  $\beta$ -CD with o-, m- and p-coumaric acids, (Kralj et al., 2009) with piperine/curcumin, (Nag et al., 2018) or with amino acids. (S.-S. Lee et al., 2018; Chen et al., 2018). Unfortunately, the aforementioned studies with complexes involving at least two molecules reported a quite low/medium mobility resolution. A high resolution IM-MS prototype using serpentine ultra-long path was described for  $\alpha$ -CD with bile acids analysis in negative and positive mode. (Chouinard et al., 2018) Very recently, a high resolution IM-MS instrument named trapped ion mobility spectrometry (TIMS) was commercially introduced. (Michelmann et al., 2015) TIMS operates at low electric field, preventing ion heating and exhibiting very high resolution. (Jeanne Dit Fouque & Fernandez-Lima, 2019; Ridgeway et al., 2018, 2019) Nevertheless, its application to carbohydrates analysis is still in infancy, although it was successfully applied for the analysis of glycosaminoglycan, (Wei et al., 2019) permethylated lacto-N-tetrasaccharides, (Pu et al., 2016) or separation of 13 isomeric trisaccharides. (Przybylski & Bonnet, 2021) In the study herein, we hypothesize that TIMS can be a useful analytical tool to both probe the influence of alkali metals on cyclo-oligosaccharides conformational modification (size/shape) in complexes, as well as to identify the sub-units orientation in supramolecular hierarchical assemblies and estimate the relative content of these last ones.

## **2. MATERIALS AND METHODS**

### **2.1. Chemicals and Materials**

$\alpha$ -,  $\beta$ - and  $\gamma$ -Cyclodextrin ( $\alpha$ -,  $\beta$ - and  $\gamma$ -CD, respectively) were kindly supplied by Wacker Chimie S.A.S. (Lyon, France). LiCl, NaCl, KCl, RbCl and CsCl alkali salts were purchased from Sigma-Aldrich (Saint-Quentin Fallavier, France).

## 2.2 Solvents

Methanol used for sample preparation was of MS grade and was purchased from VWR (West Chester, PA, USA). Water was of ultrapure quality (18.2 M $\Omega$ ).

## 2.3 Samples

Stock solutions were made at 1 mM in water and then diluted to 1  $\mu$ M in methanol/water (1:1 v/v) with or without salts (0.3  $\mu$ M) for further analysis.

## 2.4 TimsTOF™ Experiments.

We used ESI-timsTOF™ (Bruker Daltonics, Bremen, Germany) operating with oTOF control v5.0 software. The source temperature was hold at 200°C, and the drying and nebulizing gas (N<sub>2</sub>) operate at a flow rate of 3 L. min<sup>-1</sup> and at a pressure of 0.3 bar. The instrument was calibrated using Tuning Mix G24221 (Agilent Technologies, Les Ulis, France). Applied voltages were +4 kV and -0.5 kV for capillary and endplate offset, respectively. Acquisition was achieved in the  $m/z$  400-4000 range with a centre at  $m/z$  500. TIMS separation depends on the gas flow velocity ( $v_g$ ), elution voltage ( $V_{elution}$ ), ramp time ( $t_{ramp}$ ), base voltage ( $V_{out}$ ) and the electric field ( $\vec{E}$ ). The reduced mobility,  $K_0$ , can be calculated as follows:

$$K_0 = \frac{v_g}{\vec{E}} = \frac{A}{(V_{elution} - V_{out})} \text{ (Eq. 1)}$$

The mobility calibration constant  $A$  was determined using known reduced mobilities of tuning mix components. The resolving power ( $R$ ) and resolution ( $r$ ) are defined as  $R = (1/K_0)/w$  and  $r = 1.18 \times [(1/K_0)_2 - (1/K_0)_1]/(w_1 + w_2)$ , where  $w$  is the full peak width at half-maximum. To improve separation efficiency, scan rate ( $Sr = \Delta V_{\text{ramp}}/t_{\text{ramp}}$ ) was tuned thanks to imeX™ technology. For this,  $t_{\text{ramp}}$  is automatically set as function of manually adjusted  $\Delta V_{\text{ramp}}$ . N<sub>2</sub> was used as buffer gas at funnel temperature ( $T = 305$  K) with  $v_g$  set by the pressure difference of 1.69 mbar. A potential of 350 Vpp was applied to radially confine the trapped ion cloud. The measured inverse reduced mobilities were converted into collision cross sections (CCS) using the Mason-Schamp equation:

$$\Omega = \frac{(18\pi)^{1/2}}{16} \times \frac{q}{(k_B \times T)^{1/2}} \times \left[ \frac{1}{m_i} + \frac{1}{m_g} \right]^{1/2} \times \frac{1}{N} \times \frac{1}{K_0} \text{ (Eq. 2)}$$

where  $q$  is the ion charge,  $k_B$  is the Boltzmann constant,  $N$  is the gas number density,  $m_i$  is the ion mass, and  $m_g$  is the gas molecule mass. TIMS-MS spectra and mobilograms were analysed using Compass Data Analysis 5.1 (Bruker).

## 2.6 ESI-TIMS-MS analysis of the cyclo-oligosaccharides

Throughout this study, all cyclo-oligosaccharides were analysed in the positive ion mode with or without salt doping. All samples were continuously infused at 3  $\mu\text{L} \cdot \text{min}^{-1}$  via a 250 mL syringe.

## 2.7 Theoretical Collision Cross Section Calculations



All initial geometry relaxations were performed using the Merck molecular force field (MMFF94) implemented in Avogadro (v1.95.1). Geometry optimization was finalized using density functional theory (DFT) as previously described (Dossmann et al., 2021) and calculations with NWChem (v7.0). Theoretical CCS calculations were carried out in IMoS (v.1.10)(Larriba & Hogan, 2013) using the average of ten processes by Elastic/Diffuse Hard Sphere Scattering or Trajectory method Diffuse Hard Sphere Scattering.<sup>46</sup>

### 3. RESULTS AND DISCUSSION

As all neutral carbohydrates molecules, cyclodextrins exhibit intrinsically a strong affinity towards usual alkali metals.(Frański et al., 2005; Metzger et al., 1991; Przybylski et al., 2015; Przybylski & Bonnet, 2013; Reale et al., 2005) We have previously demonstrated that a solution containing an equimolar mixtures of  $\beta$ -CD and LiCl, NaCl and KCl allowed to determine apparent solution selectivity and the relative affinity of various complexes.(Przybylski et al., 2015) However, here we only aimed to study size and conformation of the complexes by IM-MS, and not the abundance. In this sense, as glassware provides enough source of  $\text{Na}^+$  and  $\text{K}^+$ , we have directly acquired a first series of spectra with separate  $\alpha$ -,  $\beta$ - and  $\gamma$ -CD without any addition. In a second series,  $\alpha$ -,  $\beta$ - or  $\gamma$ -CD was mixed with each alkali metals.

#### 3.1 Mobility of singly charged monomers

##### 3.1.1 Protonated and ammoniated native cyclodextrins

Cyclodextrins present a lower affinity for  $\text{H}^+/\text{NH}_4^+$  as compare to usual alkali metals. However, the gas phase basicity of glucose is reported to be  $188 \pm 3 \text{ kcal.mol}^{-1}$ .(Jebber et al., 1996) Hence,

even without any doping, ESI full spectra reveal the presence of such adducts coupled as singly ions at  $m/z$  973.3207/990.3494, 1135.3751/1152.4027 and 1297.4280/1314.4578 for  $\alpha$ -,  $\beta$ - and  $\gamma$ -CD, respectively (Fig. 1).

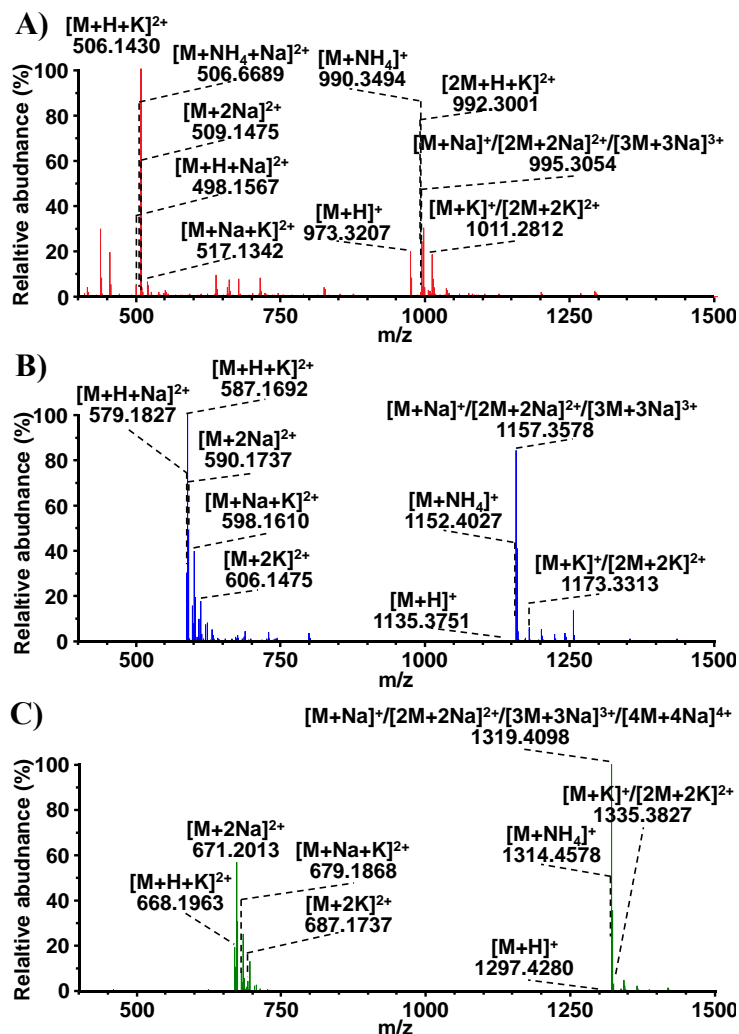


**Fig. 1.** Full MS spectra of  $\alpha$ -CD (A),  $\beta$ -CD (B) and  $\gamma$ -CD (C) without salt doping.

Examination of the respective extracted mobilograms leads to a couple of prominent/minor mobility peaks for  $\alpha$ -CD and  $\gamma$ -CD with  $1/K_0$  values of 1.365/1.389 and 1.601/1.567 V.s/cm<sup>2</sup>, respectively (Fig. 2).

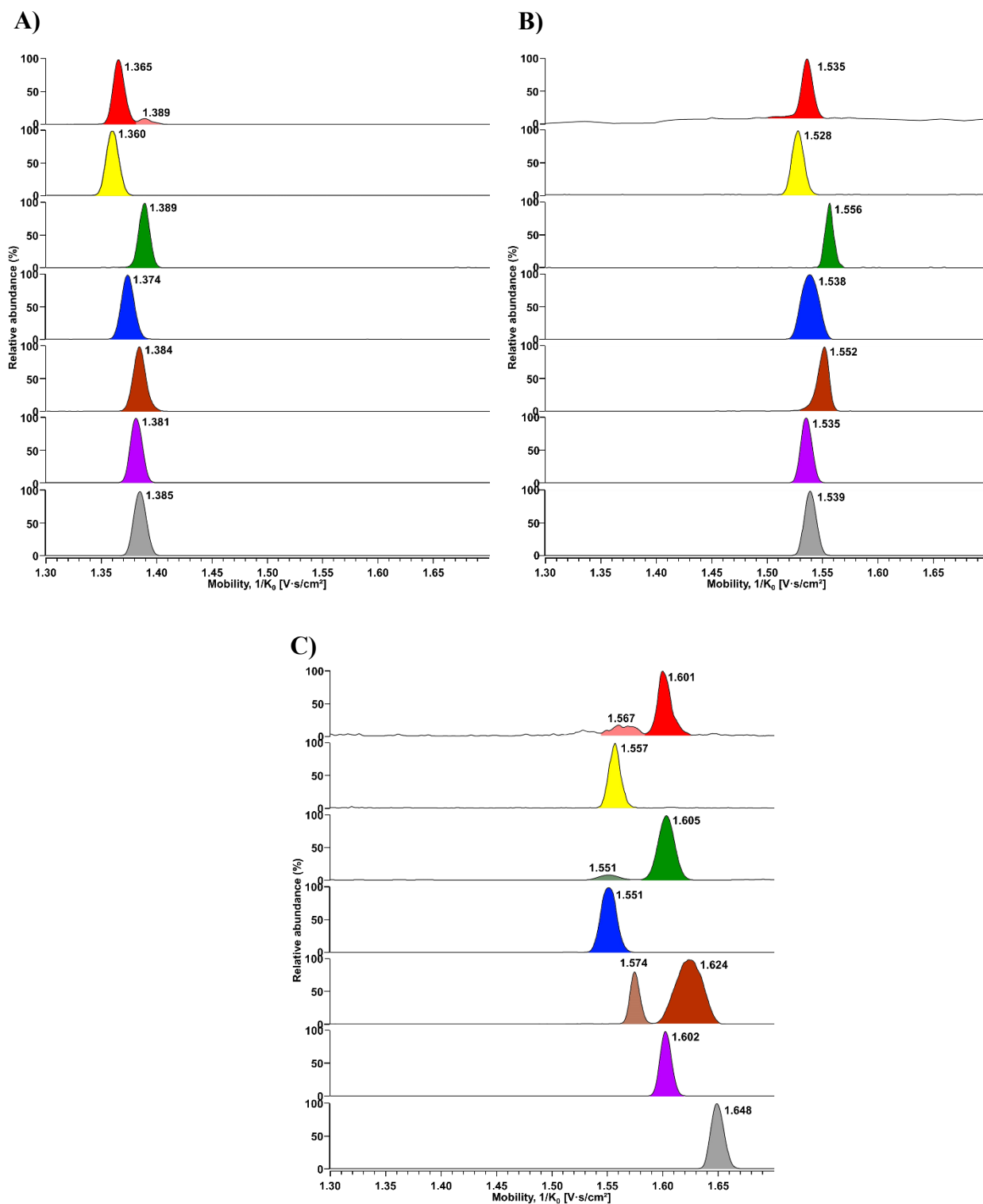


**Fig. 2.** TIMS based mobilograms for singly charged ions  $[CD+X]^+$  of A)  $\alpha$ -CD, B)  $\beta$ -CD and C)  $\gamma$ -CD.

Color coding for X: H (red), Li (yellow),  $NH_4^+$  (green), Na (blue), K (brown), Rb (violet) and Cs (grey).

Conversely,  $\beta$ -CD presents a single mobility peak at 1.535 V.s/cm<sup>2</sup> reflecting a unique stabilized location of the proton. Regarding ammoniated adducts,  $\alpha$ -/ $\beta$ -CD present a single peak with  $1/K_0$  values equal to 1.389 and 1556 V.s/cm<sup>2</sup>, respectively, while for  $\gamma$ -CD, a couple of values at 1.605/1.551 V.s/cm<sup>2</sup> were observed (Fig. 2). Such result may be explained by a more pronounced flexibility leading to two distinct complexes  $[\gamma\text{-CD}+\text{NH}_4]^+$ .

### **3.1.2 Native cyclodextrins with alkali metals (Li, Na, K, Rb and Cs)**

Native CDs exhibit lone pairs which greatly favours the attachment and stabilization of alkali metals. Mobility values of singly charged  $\alpha$ -CD gradually increase from lithium to sodium (1.360 to 1.374 V.s/cm<sup>2</sup>), and again with potassium (1.384 V.s/cm<sup>2</sup>), and then slightly decrease for rubidium (1.381 V.s/cm<sup>2</sup>) before to be barely higher with cesium (1.385 V.s/cm<sup>2</sup>) (Fig. 2). As expected, higher mobility values for  $\beta$ -CD than  $\alpha$ -CD were measured with all alkali metals. Moreover, the same increasing trend was observed for lithium, sodium and potassium (1.528, 1.538 and 1.552 V.s/cm<sup>2</sup>, respectively). Conversely, lower values than potassium were measured with rubidium and cesium (1.535 and 1.539 V.s/cm<sup>2</sup>, respectively). Regarding  $\gamma$ -CD, except higher values than  $\beta$ -CD, it can be noted a significant difference in the evolution of mobility values that the two previous CDs. If  $[\gamma\text{-CD}+\text{Li}]^+$  and  $[\gamma\text{-CD}+\text{Na}]^+$  are quasi-similar (1.557 and 1.551 V.s/cm<sup>2</sup>, respectively), at least two distinct peaks at higher mobility values were observed for  $[\gamma\text{-CD}+\text{K}]^+$  (1.624/1.539 V.s/cm<sup>2</sup>, with the latter detected as a twofold lower abundance). Similarly to  $\alpha$ -CD and as compared to main  $[\gamma\text{-CD}+\text{K}]^+$  value, mobility peak of  $[\gamma\text{-CD}+\text{Rb}]^+$  is lower (1.602 V.s/cm<sup>2</sup>) whereas that of  $[\gamma\text{-CD}+\text{Cs}]^+$  is the highest (1.648 V.s/cm<sup>2</sup>). From these data, and except for  $[\gamma\text{-CD}+\text{K}]^+$ , a single mobility peak is systematically obtained for singly charged species, presumably corresponding to a unique and stable complex.

### 3.2 Mobility of doubly charged monomers

The  $[\alpha\text{-CD}+\text{H}+\text{Na}]^{2+}$  and  $[\alpha\text{-CD}+\text{H}+\text{K}]^{2+}$  ions lead to a close mobility value of 0.798 and 0.791 V.s/cm<sup>2</sup>, respectively. With lithiated complexes ( $[\alpha\text{-CD}+\text{Li}+\text{X}]^{2+}$ ), mobility values were lower at 0.747, 0.763 and 0.759 V.s/cm<sup>2</sup>, for  $X = \text{Li}, \text{Na}$  and  $\text{K}$ , respectively. Interestingly for both  $[\alpha\text{-CD}+2\text{Na}]^{2+}$  or  $[\alpha\text{-CD}+\text{Na}+\text{K}]^{2+}$ , two couples of mobility peak were detected at 0.803/0.795 and 0.790/0.810 V.s/cm<sup>2</sup>, respectively. Such observation suggests the existence of two distinct ternary complexes for each ion. None doubly charged species based  $\alpha\text{-CD}$  involving two potassium or even one/two rubidium and cesium was detected. This is presumably due to higher ionic radii ( $r_i = 137, 152$  and  $167$  pm for  $\text{K}^+, \text{Rb}^+$  and  $\text{Cs}^+$ , respectively)(Haymes, Lide & Bruno, 2016) impairing a good matching, with the coordination sites from this cyclo-oligosaccharide template. As expected, the mobility values  $[\beta\text{-CD}+\text{H}+\text{X}]^{2+}$  with  $X = \text{Na}$  and  $\text{K}$  are higher than for  $\alpha\text{-CD}$ . Nevertheless, no significant differences occurs for the two herein  $\beta\text{-CD}$  species with 0.854 and 0.855 V.s/cm<sup>2</sup>, respectively. Such results show that  $[\beta\text{-CD}+\text{H}+\text{K}]^{2+}$  as compact as  $[\beta\text{-CD}+\text{H}+\text{Na}]^{2+}$  suggesting similar coordination sites and/or flexibility of the CD. Introduction of lithium in ternary complex leads to a single mobility peak at 0.801, 0.814 and 0.830 V.s/cm<sup>2</sup>, for  $[\beta\text{-CD}+2\text{Li}]^{2+}$ ,  $[\beta\text{-CD}+\text{Li}+\text{Na}]^{2+}$  and  $[\beta\text{-CD}+\text{Li}+\text{K}]^{2+}$ , respectively. Similarly, to  $\alpha\text{-CD}$ , for adducts with 2Na and 1Na+K, two couples of mobility peaks were observed at 0.852/0.820 and 0.828/0.851 V.s/cm<sup>2</sup>, respectively. Interestingly, the  $\beta\text{-CD}$  allows the formation of both  $[\beta\text{-CD}+2\text{X}]^{2+}$  with  $X = \text{K}$  or  $\text{Rb}$  exhibiting two distinct mobility values (0.869/0.839 V.s/cm<sup>2</sup>) for the former and a unique for the latter (0.876 V.s/cm<sup>2</sup>). Concerning  $\gamma\text{-CD}$ , as for  $\beta\text{-CD}$ , only a single peak was observed for  $[\gamma\text{-CD}+2\text{Li}]^{2+}$ ,  $[\gamma\text{-CD}+\text{Li}+\text{Na}]^{2+}$ ,  $[\gamma\text{-CD}+\text{Li}+\text{K}]^{2+}$ ,  $[\gamma\text{-CD}+\text{Na}+\text{Rb}]^{2+}$  and  $[\gamma\text{-CD}+2\text{Rb}]^{2+}$  at 0.826, 0.852, 0.873, 0.900 and 0.878 V.s/cm<sup>2</sup>, respectively. Nonetheless, instead of a unique peak for  $\beta\text{-CD}$ ,  $[\gamma\text{-CD}+\text{H}+\text{Na}]^{2+}$  and

$[\gamma\text{-CD} + \text{K} + \text{Rb}]^{2+}$ , showed two peaks at 0.903/0.879 and 0.892/0.915 V.s/cm<sup>2</sup>, respectively. As regards other doubly charged species, very different behaviours were quoted out for  $\gamma\text{-CD}$  compare to both  $\alpha\text{-}$  and  $\beta\text{-}$  ones. Indeed, three distinct peaks were detected for  $[\gamma\text{-CD} + \text{X} + \text{K}]^{2+}$  with  $\text{X} = \text{H}$  or  $\text{K}$  at 0.873/0.907/0.847 and 0.897/0.855/0.876 respectively. For  $[\gamma\text{-CD} + \text{Na} + \text{X}]^{2+}$  with  $\text{X} = \text{Na}$  or  $\text{K}$ , only one value can be observed at 0.893 and 0.866 V.s/cm<sup>2</sup>, respectively. Conversely to  $\alpha\text{-}/\beta\text{-CDs}$ , complexes involving cesium have been successfully detected for  $\gamma\text{-CD}$  with only one value for  $[\gamma\text{-CD} + \text{Na} + \text{Cs}]^{2+}$  (0.901 V.s/cm<sup>2</sup>) and  $[\gamma\text{-CD} + 2\text{Cs}]^{2+}$  (0.882 V.s/cm<sup>2</sup>) and three for  $[\gamma\text{-CD} + \text{K} + \text{Cs}]^{2+}$  (0.876/0.890/0.899 V.s/cm<sup>2</sup>). These last results support the hypothesis that  $\beta\text{-CD}$  is the smaller CD able to simultaneously attach two potassium. Also, a minimal number of 7 and 8 glucoses is required to complex two simultaneous potassium and rubidium or cesium based doubly charged species, respectively. Moreover, it was previously observed that the coulombic repulsion between two cations in the ternary complex is reduced for the larger size host. (Wang et al., 2010) Furthermore, two, three and even four mobility peaks can be detected for a given doubly charged ion. That strongly suggests the simultaneous occurrence of several more and less stable complex, which can be estimated by area integration of mobility peaks.

### **3.3 Scaling cyclodextrin/metals complexes using the collision cross section as molecular descriptor**

After determination of ion mobility values of a given ion and by using Mason-Schamp equation (see experimental section), its collision cross section (CCS) can be deducted. The relationship between structure and CCS has been widely used to offer insights into the structures of gas phase species. More particularly, CCS provide precious pieces of information regarding size and shape of the corresponding molecules. In the case of CDs, we used IM-MS to probe both size difference

informing on location of coordination site including more and less deep insertion in the cavity, and on the shape feature which can be due to the existence of various conformational states during cationization.

### **3.3.1 Singly charged ions**

Protonated  $\alpha$ -,  $\beta$ - and  $\gamma$ -CD have  $CCS_{N_2}$  equal to 276.8/282.2, 311.1 and 323.8/317.2  $\text{\AA}^2$ , respectively. Herein values are very close to those reported in the literature (Table 1). (Klein et al., 2018; May et al., 2014) Nonetheless, we noted that herein,  $\alpha$ - and  $\gamma$ -CD exhibits two and three distinct mobility peaks respectively, which can be putatively ascribed to different conformational states or protomers. This was obtained thanks to the high resolution of TIMS while unique value was extracted from DTIMS analysis. (Klein et al., 2018) Regarding ammonium adducts, an increase of CCS according to size was observed with 282.1, 315.4 and 324.4/313.9  $\text{\AA}^2$  for  $\alpha$ -,  $\beta$ - and  $\gamma$ -CD, respectively. However, we noted none linearly correlation since we could expect 348.7  $\text{\AA}^2$  for a not deformed  $\gamma$ -CD, but obtained values lower by  $\sim 24$ -30  $\text{\AA}^2$ . From these last results, two hypotheses can be formulated either ammonium ion can be more deeply inserted into the  $\gamma$ -CD cavity and/or  $\gamma$ -CD can adopt deformed conformations due to its intrinsic flexibility. In all case, the comparison of any given ion form as a function of CD type shows an expected increase in CCS as a function of increasing molecular weight and/or size (e.g. with  $[M+Li]^+$ , CSS is 276.1, 309.6 and 315.1  $\text{\AA}^2$  for  $\alpha$ -,  $\beta$ - and  $\gamma$ -CD, respectively (Table 1 and Fig. S1).

**Table 1.** Characteristics of singly charged ions from  $\alpha$ -,  $\beta$ - and  $\gamma$ -CD under alkali-metal cation complexes. Brackets indicate the relative content. \*: large peak, ND: not detected; NC: not calculated.

Name	<i>m/z</i>		Mass accuracy (ppm)	1/ <i>K</i> <sub>0</sub> (V.s.cm <sup>-2</sup> )	CCS <sub>N2</sub> (Å <sup>2</sup> )		
	Experimental	Theoretical			Experimental (n=5)	Theoretical (n=10)	Literature
[ $\alpha$ -CD+H] <sup>+</sup>	973.3207	973.3242	-3.6	1.365 /1.389 (92/8)	276.8±0.6/282.2±0.5	276.8±0.8/281.8±0.7	280.5 <sup>a</sup> ;285.2 <sup>b</sup>
[ $\alpha$ -CD+Li] <sup>+</sup>	979.3346	979.3325	2.2	1.360	276.1±0.4	276.3±0.6	
[ $\alpha$ -CD+NH <sub>4</sub> ] <sup>+</sup>	990.3494	990.3508	-1.4	1.389	282.1±0.7	282.2±0.8	280.9 <sup>a</sup>
[ $\alpha$ -CD+Na] <sup>+</sup>	995.3054	995.3062	-0.8	1.374	278.9±0.4	278.8±0.5	278.2 <sup>a</sup> ;285.5 <sup>b</sup>
[ $\alpha$ -CD+K] <sup>+</sup>	1011.2812	1011.2801	1.1	1.384	281.0±0.5	280.9±0.6	280.0 <sup>a</sup> ;287.7 <sup>b</sup>
[ $\alpha$ -CD+Rb] <sup>+</sup>	1057.2269	1057.2282	-1.2	1.381	280.2±0.8	280.2±0.8	
[ $\alpha$ -CD+Cs] <sup>+</sup>	1105.2208	1105.2218	-0.9	1.385	280.8±0.9	281.2±0.8	
[ $\beta$ -CD+H] <sup>+</sup>	1135.3751	1135.3770	-1.7	1.535	311.1±0.4	311.5±0.6	312.4 <sup>a</sup> ; 301.3/319.6 <sup>b</sup>
[ $\beta$ -CD+Li] <sup>+</sup>	1141.3843	1141.3853	-0.9	1.528	309.6±0.6	309.9±0.8	
[ $\beta$ -CD+NH <sub>4</sub> ] <sup>+</sup>	1152.4027	1152.4036	-0.8	1.556	315.4±1.1	315.3±0.6	312.5 <sup>a</sup>
[ $\beta$ -CD+Na] <sup>+</sup>	1157.3578	1157.3590	-1.0	1.538	311.7±0.6	311.8±0.4	309.0 <sup>a</sup> ;319.7 <sup>b</sup>
[ $\beta$ -CD+K] <sup>+</sup>	1173.3313	1173.3329	-1.4	1.552	314.4±0.7	314.6±0.7	308.9 <sup>a</sup> ;320.3 <sup>b</sup>
[ $\beta$ -CD+Rb] <sup>+</sup>	1219.2796	1219.2810	-1.2	1.535	310.9±0.6	311.2±1.0	
[ $\beta$ -CD+Cs] <sup>+</sup>	1267.2733	1267.2747	-1.1	1.539	311.5±0.8	311.3±1.1	
[ $\gamma$ -CD+H] <sup>+</sup>	1297.4280	1297.4299	-1.4	1.601/1.567 (81/19)	323.8±0.8/317.2±0.9	323.6±0.7/317.3±0.9	324.3 <sup>a</sup> ;322.6 <sup>b</sup>
[ $\gamma$ -CD+Li] <sup>+</sup>	1303.4372	1303.4382	-0.7	1.557	315.1±0.6	314.9±0.5	317.7 <sup>b</sup>
[ $\gamma$ -CD+NH <sub>4</sub> ] <sup>+</sup>	1314.4578	1314.4564	1.1	1.605/1.551 (93/7)	324.4/313.9±0.7	324.3±0.9/314.0±1.3	324.3 <sup>a</sup> ;
[ $\gamma$ -CD+Na] <sup>+</sup>	1319.4098	1319.4118	-1.5	1.551	313.9±0.8	313.8±1.0	316.0 <sup>a</sup> ;322.1 <sup>b</sup>
[ $\gamma$ -CD+K] <sup>+</sup>	1335.3827	1335.3857	-2.3	1.624*/1.574 (77/23)	328.5±0.8/318.8±1.2	328.8±1.1/318.6±1.2	319.3 <sup>a</sup> ;324.8 <sup>b</sup>
[ $\gamma$ -CD+Rb] <sup>+</sup>	1381.3364	1381.3383	-1.4	1.602	324.0±1.0	324.0±1.3	327.3 <sup>b</sup>
[ $\gamma$ -CD+Cs] <sup>+</sup>	1429.3258	1429.3275	-1.2	1.648	333.3±1.1	333.2±1.3	338.2 <sup>b</sup>

<sup>a</sup> Klein et al., 2018

<sup>b</sup> May et al., 2014

Further examination of complexes involving alkali metals, allows achievement of some observations: i) with  $\alpha$ -CD, CCS increase linearly by step of 2.8 and 2.1 Å<sup>2</sup> from Li<sup>+</sup> to Na<sup>+</sup> and from Na<sup>+</sup> to K<sup>+</sup>, respectively, and then remains quite constant with Rb<sup>+</sup> and Cs<sup>+</sup> (Fig. S1, red star) ii) with  $\beta$ -CD, CCS increase linearly also by step of 2.1 and 2.7 Å<sup>2</sup> from Li<sup>+</sup> to Na<sup>+</sup> and from Na<sup>+</sup> to K<sup>+</sup>, respectively, but decrease by ~3.5 Å<sup>2</sup> for Rb<sup>+</sup> and drop only slightly for Cs<sup>+</sup> (Fig. S1, blue square). iii) with  $\gamma$ -CD, measured CCS portray a completely different behaviour as a slight decrease by ~1.2 Å<sup>2</sup> occurred from Li<sup>+</sup> to Na<sup>+</sup> and then a drop by 4.9 or 14.6 Å<sup>2</sup> for K<sup>+</sup> as two peaks were detected. Next, according to previous considered values for K<sup>+</sup> a variation of -4.5/+5.2 Å<sup>2</sup> occurred for Rb<sup>+</sup> and a drop by 9.3 Å<sup>2</sup> from this last one to Cs<sup>+</sup> (Fig. S1, green circle). Also, such a decrease in CCS observed with



CDs and some alkali metals compared to corresponding protonated or ammoniated forms, can be tentatively explained by a greater oxophilicity - stronger coordination of the formers, as previously described for carbohydrates. (Fenn & McLean, 2011) In brief, CCS can be summarized as a consequence of a balance between main factors: size of both cation and CD (including eventual distortions) and more and less deep inclusion of the cation inside cavity (according to coordination features).

### 3.3.2 Doubly charged ions

Considering the sum of the relative intensities from all alkali metal cations-based CDs observed by MS, the part of 1:2 complexes compared with 1:1 one increased constantly from  $\alpha$ -CD to  $\gamma$ -CD. Such trend was similar to that reported elsewhere for an increasing methylation degree on  $\beta$ -CD. (Przybylski et al., 2015) As for singly charged species, any particular ternary complexes the higher the molecular weight and/or size of CD, the higher the CCS (e.g. with  $[M+2Li]^{2+}$ , 307.6, 328.6 and 337.9  $\text{\AA}^2$  for  $\alpha$ -,  $\beta$ - and  $\gamma$ -CD, respectively) (Table S1 and Fig. 3).

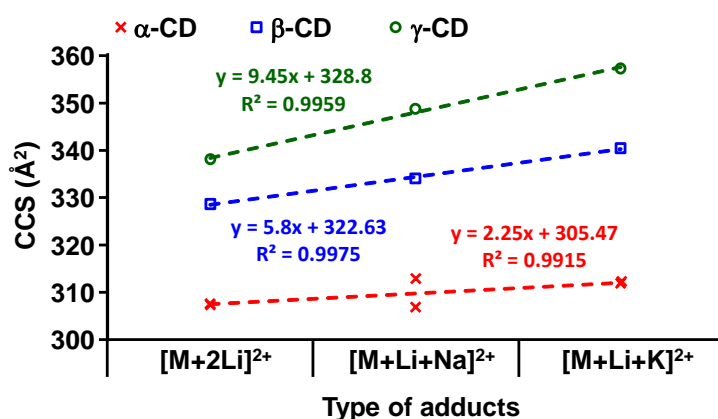


**Fig.3.** Evolution of CCS as function of doubly charged species  $[CD+Li+X]^{2+}$  where X is lithium, sodium or potassium.  $\alpha$ -CD (red cross),  $\beta$ -CD (blue square) and  $\gamma$ -CD (green circle).

Also, interestingly, for a given CD involving both one lithium and in the other hand an additional lithium, sodium or potassium, CCS increase linearly with the size of the associated cation. Examination of the slope value of the resulting curve i.e. 2.25, 5.8 and 9.45 portrays a growing amplitude in CCS drop for  $\alpha$ -,  $\beta$ - and  $\gamma$ -CD, respectively (Fig. 3). However, such behaviour according size of the cations was not obvious for all ternary complexes, even if a relative growing linearity of CCS can be deducted for  $[\alpha\text{-CD or } \beta\text{-CD} + \text{Na} + \text{X}]^{2+}$  and  $[\alpha\text{-CD or } \beta\text{-CD} + \text{K} + \text{X}]^{2+}$  (where  $X = \text{Li, Na and K}$ ) as well as for  $[\gamma\text{-CD} + \text{K} + \text{X}]^{2+}$   $[\gamma\text{-CD} + \text{Na} + \text{X}]^{2+}$  (where  $X = \text{Li, Na, K and Rb}$ ) (Fig. S2-S5). We have previously demonstrated by molecular modeling that two cations are stabilized by various coordination sites onto the primary rim of  $\beta$ -CD.(Przybylski et al., 2015) For example, ternary complexes with native  $\beta$ -CD including 2 Li are stabilized each one by three electron donating. Such coordination landscape involves 3 oxygens of the primary rim of  $n$ ,  $n+1$  and  $n+3$  glucose for one side and  $n-1$ ,  $n-2$  and  $n-3$  for the second side.(Przybylski et al., 2015) The lower bond length between the three proximal oxygens of doubly lithiated forms highlighted a tighter interaction of the two metals than for corresponding singly charged complexes. Moreover, the coordination of two cations induces a strong distortion of CDs like a spindle with cation localized at each tip. Increasing CCS can be roughly visualized using Van der Waals (VDW) radii for each atom of the molecule, in other words VDW surface through which the molecule might be conceived as interacting with other ones. Examples of VDW surface were given for the three axis of  $[\beta\text{-CD} + \text{Li} + \text{X}]^{2+}$  (where  $X = \text{Li, Na or K}$ ) (Fig. 4).

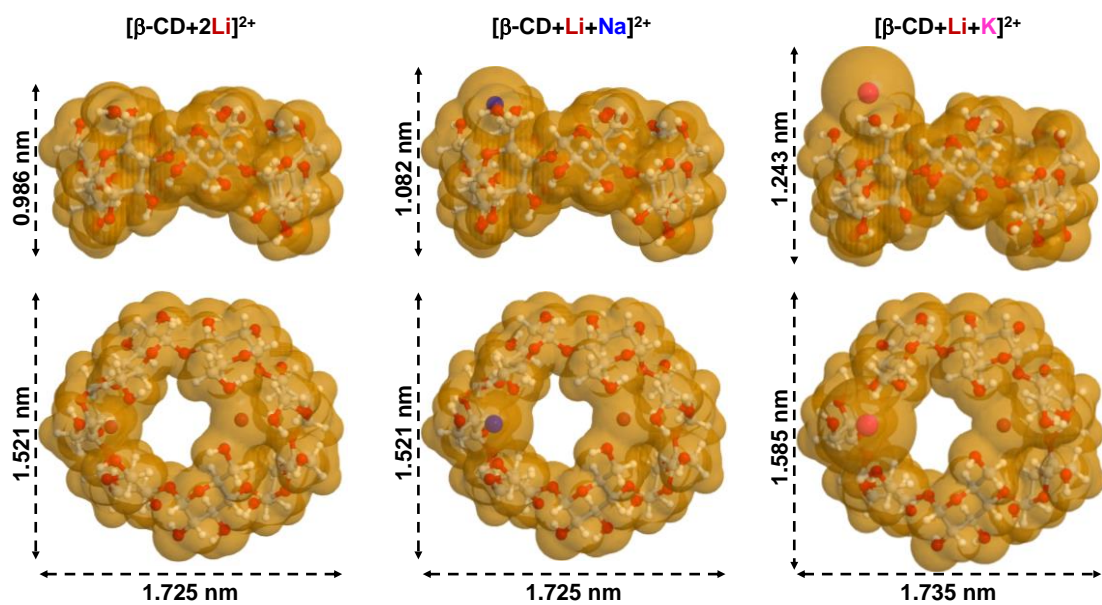


**Fig. 4.** Van der Waals surface of  $[\beta\text{-CD}+\text{Li}+\text{X}]^{2+}$  (where  $\text{X} = \text{Li}, \text{Na}$  or  $\text{K}$ ) from ball and stick model of optimized models of complexes with x,y axis (bottom view) and z-axis side (top view).

Such last examples depict well the possible differences portraying the linear increase of the CCS values where only length on the z axis increases while those of x, y axis remain constant from  $[\beta\text{-CD}+\text{Li}+\text{Li}]^{2+}$  to  $[\beta\text{-CD}+\text{Li}+\text{Na}]^{2+}$  and then length of the three axis enlarge from  $[\beta\text{-CD}+\text{Li}+\text{Na}]^{2+}$  to  $[\beta\text{-CD}+\text{Li}+\text{K}]^{2+}$ .

### 3.4 Study of multimeric assemblies of cyclodextrins

Literature described that CD can form aggregates with various shapes but based on only 2 types of molecular arrangements: clustered cage or channel.(Saenger et al., 1998) Nevertheless, probability to form disordered assemblies prevails from concentration in the millimolar

range.(Messner et al., 2010) Nevertheless, in our study, we used diluted solution (one micromolar) which must favour formation of ordered assemblies. All the CD have the shape of a basketball net, including a large (head, H) and a small (tail, T) aperture. In tubular arrangements of CDs, they can interact among themselves according to three possible orientations: Head-to-Tail (H•T), Head-to-Head (H•H) or Tail-to-Tail, (T•T).(Staelens et al., 2015) Such organization is the result of the formation of several intermolecular hydrogen bonds constituting the main driving force for holding and stabilizing two or more units together.(Nascimento et al., 2005) As example, we have investigated the ion mobility traces of the singly charged ion at  $m/z$  1967.6199 ascribed to  $[(\alpha\text{-CD})_2+\text{Na}]^+$  and deduced corresponding CCS values (Fig. 5).

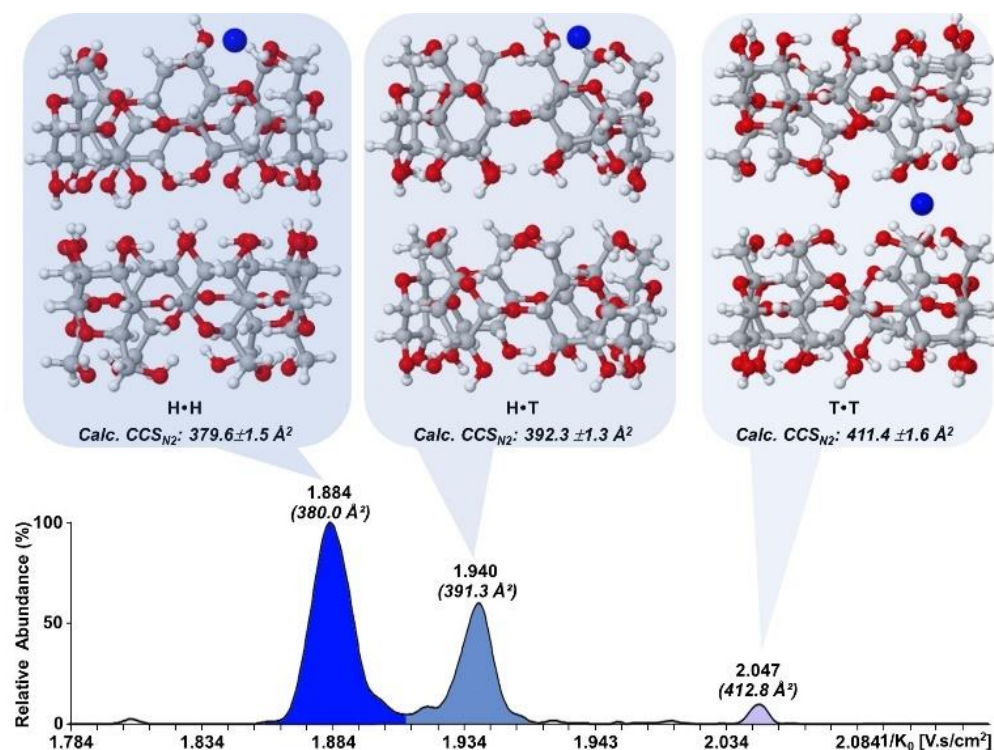


**Fig. 5.** TIMS based mobilogram for the singly charged dimer of  $\alpha$ -CD  $[(\alpha\text{-CD})_2+\text{Na}]^+$  revealing the three orientations as H•H (bright k blue), H•T (steel blue) and T•T (clear blue).

Examination of the mobilogram revealed two main peaks at 380.0 and 391.3 Å<sup>2</sup> and one minor one at 412.8 Å<sup>2</sup>. These values are in very good agreement with theoretical CCS calculated for H•H (379.6±1.5 Å<sup>2</sup>), H•T (392.3 ±1.3 Å<sup>2</sup>), and T•T (411.4±1.6 Å<sup>2</sup>) assemblies, respectively. Such results demonstrated that TIMS can successfully discriminate the three possible orientations of mono-sodiated dimers of CDs. Efficiency of separation can be defined with resolving power (*R*) of a given mobility peak and also with peak-to-peak resolution (*r*). Here, the values were equal to 109/141/282 and 1.8/5.1 depicting both high *R* and *r*. Also, by approximating that equal ionization efficiencies take place and that relative abundance of the overall spectrum could be interpreted as a good image of the solution content, we can estimate content of mono-sodiated species of H•H, H•T and T•T α-CD dimers as 59, 35 and 6%, respectively. Such content is in good agreement with stability order obtained from molecular dynamics (MD) simulations (T•T < H•T < H•H). (Bonnet et al., 2001) Regarding doubly charged species with the two same cations, the nature of the cation leads to contrasted results in terms of both *r* and *R*, which rely on their ability to detect and also to discriminate the different orientations as well as their respective content. Results for [(α-CD)<sub>2</sub>+2X]<sup>2+</sup> with X=Li, Na, K, Rb or Cs were given in Fig. 6.

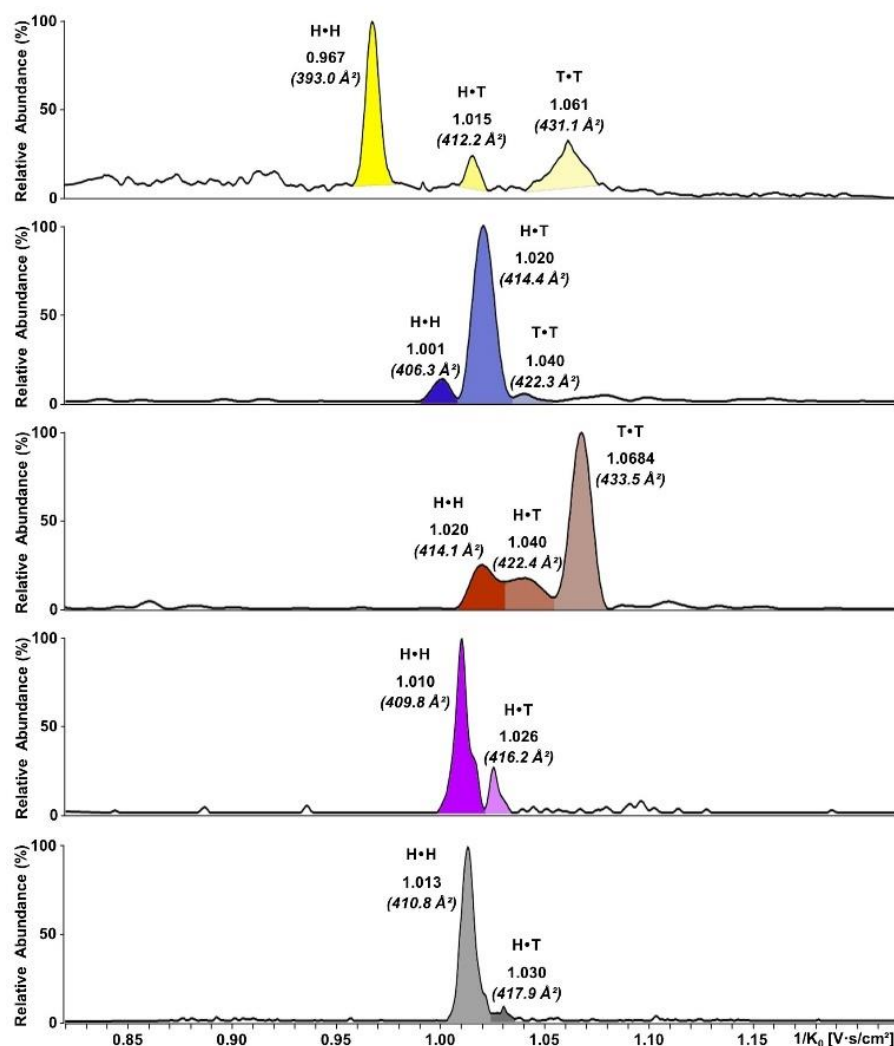
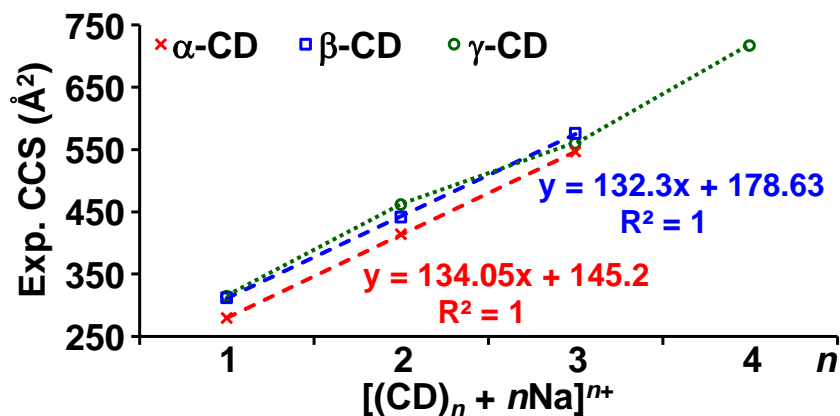


**Fig. 6.** TIMS based mobilograms for the doubly charged dimer of  $\alpha$ -CD ( $[(\alpha\text{-CD})_2X]^{2+}$ ) revealing the possible orientations (H•H, H•T and T•T). Color coding for X: Li (yellow), Na (blue), K (brown), Rb (violet) and Cs (grey).

In details, double adduction with lithium allows to easily highlight the presence of the three possible orientations (H•H, H•T and T•T) of  $\alpha$ -CD dimer with both  $R$  equal to 138, 127 and 71, respectively, and  $r$  of 3.2 (H•H to H•T) and 2.0 (H•T to T•T). With two sodium or two potassium,  $r$  strongly decreases to 0.8/1.0 and 0.5/0.8 for H•H to H•T/H•T to T•T, respectively. The same trend

383 was noted regarding  $R$  with values for the mobility peak of the three orientations of 80/85/145  
 384 and 65/47/92, respectively. Introduction of rubidium lead to detection of only two orientations  
 385 i.e. H•H and H•T with satisfactory  $R$  (141/174) and  $r$  (1.2). Such data strongly suggest that the T•T  
 386 dimer of  $[(\alpha\text{-CD})_2+2\text{Rb}]^{2+}$  cannot be formed and/or stabilized in the gas phase. Similar results  
 387 were obtained with cesium leading to the two dimers: H•H and H•T with close  $R$  (133/138) and  $r$   
 388 (1.1), and a lesser content of the latter orientation as compared to Rb (9 vs 22%). Interestingly,  $R$   
 389 and  $r$  from  $[(\alpha\text{-CD})_2+2\text{Na}]^{2+}$  are both lower than  $[(\alpha\text{-CD})_2+\text{Na}]^+$  (109/141/282 vs 80/85/145 and  
 390 0.8/1.0 vs 1.8/5.1). Moreover, difference in CCS of the latter vary from 11.3 Å<sup>2</sup> and 21.5 Å<sup>2</sup> for  
 391 H•H to H•T and H•T to T•T, respectively, while it is constant (8 Å<sup>2</sup>) for the former. Such results  
 392 support the hypothesis that the presence of two sodium acts as a more structuring agent than  
 393 only one, presumably by compacting dimer to minimize natural intrinsic difference resulting from  
 394 the different orientations. We have demonstrated that for a given CD, the type of adducted cat-  
 395 ions strongly influences the discrimination ability, but a given cation do not act with the same  
 396 beneficial/detrimental balance according to the studied CD. For example, the smallest alkali  
 397 metal studied herein, lithium led to the high-resolution during analysis of  $[(\alpha\text{-CD})_2+2\text{Li}]^{2+}$  (Fig. 6),  
 398 while  $[(\beta\text{-CD})_2+2\text{Li}]^{2+}$  and  $[(\gamma\text{-CD})_2+2\text{Li}]^{2+}$  only revealed two dimers namely H•H and H•T exhibiting  
 399  $R$  equal to 124/88 and 160/123, respectively, but also with  $r$  of 3.5 and 2.1, respectively (Fig. S6).  
 400 Conversely, with the largest studied alkali metal, cesium,  $[(\alpha\text{-CD})_2+2\text{Cs}]^{2+}$  exhibits only H•H and  
 401 H•T dimers ( $R$ : 133/138 and  $r$ : 1.1) while the analysis of  $[(\beta\text{-CD})_2+2\text{Cs}]^{2+}$  unambiguously showed  
 402 the presence of the three possible orientations H•H, H•T and T•T ( $R$ : 286:82/129 and  $r$ : 1.4/1.3)  
 403 respectively (Fig. S7). Finally, a single peak with an important tailing, leading to low  $R$  (96), was  
 404 obtained for  $[(\gamma\text{-CD})_2+2\text{Cs}]^{2+}$ . Such peak was mainly ascribed to H•T by computational methods,

and the tailing is presumably due to the detection and/or separation difficulty of the other dimers, due to aforementioned high distortion ability of  $\gamma$ -CD and existence of several conformers. To explore the influence of the number ( $n$ ) of CDs/charge state couple on the formation of small oligomers, we draw experimental CCS as function of  $[(CD)_n + nNa]^{n+}$  (Fig. 7).

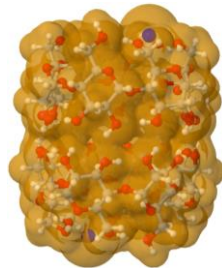
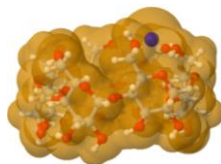


**Fig. 7.** Evolution of the experimental collision cross section as a function of  $[(CD)_n + nNa]^{n+}$  ions where  $n$  is both the number of CDs, the number of adducted sodium and the charge state.  $\alpha$ -CD (red cross),  $\beta$ -CD (blue square) and  $\gamma$ -CD (green circle).

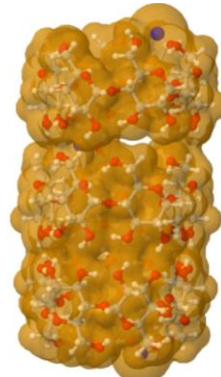
In the case of a non-driven CDs aggregation, resulting CCS should be randomly distributed. Conversely, in the case of well-ordered supramolecular assemblies with a tubular topology assimilated to a cylinder or a compact near-spherical nucleation, expected CCS fitting should be near a fully linear or involving a modular exponentiation. (Hanozin et al., 2019; Ruotolo et al., 2008) Herein, we obtain a linear fit for  $\alpha$ - and  $\beta$ -CD for 1- to 3-mer portraying both a well-organized into a hierarchical assemblies consecutive to stacked CDs and a structuring role of sodium. Such observations were confirmed by theoretical CCS calculation of single CDs and their supramolecular assemblies (Fig. 8A-B).



A)

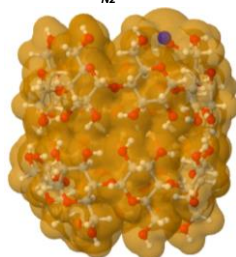
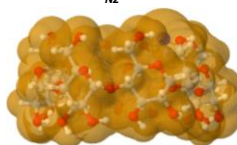
 $\alpha$ -CDExp.  $CCS_{N_2}$ :  $278.9 \pm 0.3 \text{ \AA}^2$   
Calc.  $CCS_{N_2}$ :  $278.3 \pm 0.5 \text{ \AA}^2$ Exp.  $CCS_{N_2}$ :  $414.0 \pm 1.8 \text{ \AA}^2$   
Calc.  $CCS_{N_2}$ :  $416.4 \pm 1.5 \text{ \AA}^2$ Exp.  $CCS_{N_2}$ :  $547.0 \pm 2.2 \text{ \AA}^2$   
Calc.  $CCS_{N_2}$ :  $543.9 \pm 1.9 \text{ \AA}^2$ 

H•H

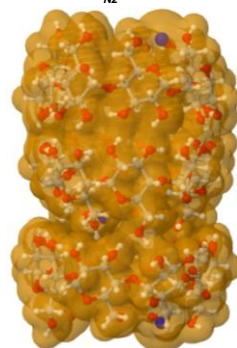


H•HT•H

B)

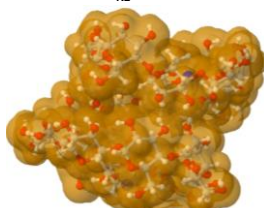
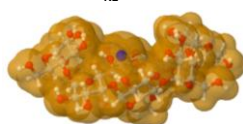
 $\beta$ -CDExp.  $CCS_{N_2}$ :  $311.7 \pm 2.7 \text{ \AA}^2$   
Calc.  $CCS_{N_2}$ :  $311.8 \pm 1.1 \text{ \AA}^2$ Exp.  $CCS_{N_2}$ :  $441.5 \pm 3.0 \text{ \AA}^2$   
Calc.  $CCS_{N_2}$ :  $437.9 \pm 1.9 \text{ \AA}^2$ Exp.  $CCS_{N_2}$ :  $571.2 \pm 3.1 \text{ \AA}^2$   
Calc.  $CCS_{N_2}$ :  $575.0 \pm 2.4 \text{ \AA}^2$ 

H•H

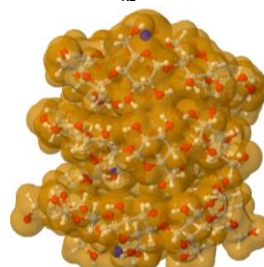


H•HT•H

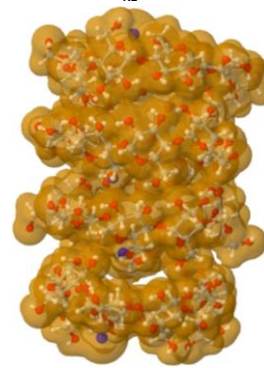
C)

 $\gamma$ -CDExp.  $CCS_{N_2}$ :  $313.9 \pm 0.8 \text{ \AA}^2$   
Calc.  $CCS_{N_2}$ :  $313.8 \pm 1.0 \text{ \AA}^2$ Exp.  $CCS_{N_2}$ :  $471.8 \pm 1.4 \text{ \AA}^2$   
Calc.  $CCS_{N_2}$ :  $473.6 \pm 2.0 \text{ \AA}^2$ Exp.  $CCS_{N_2}$ :  $560.6 \pm 2.2 \text{ \AA}^2$   
Calc.  $CCS_{N_2}$ :  $559.4 \pm 2.7 \text{ \AA}^2$ Exp.  $CCS_{N_2}$ :  $718.0 \pm 2.8 \text{ \AA}^2$   
Calc.  $CCS_{N_2}$ :  $721.3 \pm 3.0 \text{ \AA}^2$ 

H•T



H•TH•T



H•TH•TH•T

**Fig. 8.** Illustration of the incremental construction of the cyclodextrins based tubular assemblies.

Van der Waals surface from Ball and stick model of optimized models (A)  $[(\alpha\text{-CD})_n + n\text{Na}]^{n+}$ , (B)  $[(\beta\text{-CD})_n + n\text{Na}]^{n+}$  and (C)  $[(\gamma\text{-CD})_n + n\text{Na}]^{n+}$  (where  $n = 1, 2, 3$  or  $4$  for mono-, di-, tri and tetramer). Experimental ( $n=5$ ) and theoretical ( $n=10$ ) collision cross section are indicated above structures.

446  $\gamma$ -CD and its short oligomers containing until 4 units show a different behaviour. Firstly, based on  
 447 a semi-rigid conformation behaviour similar to  $\alpha$ - and  $\beta$ -CD, expected CCS of  $[\gamma\text{-CD}+\text{Na}]^+$  should  
 448 be  $\approx 348.7 \text{ \AA}^2$ , but an experimental value of  $313.8 \pm 1.0 \text{ \AA}^2$  was obtained. Such discrepancy can be  
 449 tentatively explained by a distortion of  $\gamma$ -CD. Indeed, it was mentioned in literature that when  
 450 size of CD increase, probabilities of band flip and kinks occurrence are growing. (Jacob et al., 1999;  
 451 Saenger, 1980; Steiner & Saenger, 1998) In this sense, MD simulations have previously given ev-  
 452 idences that  $\gamma$ -CD exhibits two diametrically opposed glucoses (between  $n$  and  $n \pm 4$  unit), which  
 453 are flipped by  $\sim 180^\circ$ , leading to elliptical and curved structures with a quite narrow, slit-like cav-  
 454 ity. (Bonnet et al., 2001, 2002; Suárez & Díaz, 2017) Based on the model from Bonnet *et*  
 455 *al.*, (Bonnet et al., 2001, 2002) three glucoses are folded toward the cavity leading to the for-  
 456 mation of intramolecular  $\text{O6}-\text{H6} \cdots \text{O6}$  by their corresponding primary hydroxyl groups. Such ori-  
 457 entation of some groups from the primary rim strongly supports the coordination of the sodium  
 458 cation (Fig. 8C). Secondary, slope between 2 and 3 CD is lower than that observed between both  
 459 1 to 2 and 3 to 4 CDs (Fig. 7). Similar trends were observed for  $[(\text{CD})_n + nX]^{n+}$  with  $X = \text{Li}, \text{K}$  and  $\text{Rb}$   
 460 (Fig. S8-S10). Interestingly one exception occurred for  $[(\gamma\text{-CD})_n + n\text{Cs}]^{n+}$  where a linear fit can be  
 461 calculated from mono to tetramer, presumably to a more structuring role of Cs during nanotubes  
 462 formation (Fig. S11). As previously observed, the most stable dimer was assigned to  $\text{H} \bullet \text{H}$  assem-  
 463 bly whatever CD. (Bonnet et al., 2001) Differently to  $\alpha$ - and  $\beta$ -CD, due to the incurved ellipsoidal  
 464 conformation of  $\gamma$ -CD, such dimer corresponds to superimposed irregular bowls with slightly dif-  
 465 ferent orientation of  $\sim 90^\circ$  along  $z$  axis close to structure reported by Bonnet *et al.* (Bonnet et al.,  
 466 2001) Moreover, such structural arrangement favours a closer contact between each CD and en-  
 467 hances the inter-oligosaccharides van der Waals' stabilization. Furthermore, previous studies

have demonstrated that favourable elongation of  $\gamma$ -CD based tubular arrangements corresponds to a decrease of the potential energy value of the tubes per CD unit as a function of the number of CDs.(Staelens et al., 2015) The important flexibility of  $\gamma$ -CD leads to a more compressed stacked assembly during the trimer formation compared to  $\alpha$ - and  $\beta$ -CD where a quite more incremental addition of monomer of semi-rigid structure seems to take place. Such phenomenon can explain why the CCS difference between di- ( $H\bullet H$ ) and trimer ( $H\bullet TH\bullet T$ ) is by far lower than from mono- to dimer. Then starting for a compressed trimer, an additional  $\gamma$ -CD can be associated leading to an orientated growing of the supramolecular chain by formation of a 4-mer ( $H\bullet TH\bullet TH\bullet T$ ). Interestingly, slope of the curve between CCS of 3-mer and 4-mer is strictly identical than that between 1-mer to 2-mer suggesting a similar assembly elongation process.

#### 4. CONCLUSIONS

It was unambiguously demonstrated in this work that hyphenation with high resolution TIMS represents a powerful and suitable tool to differentiate various non covalent complexes between  $\alpha$ -,  $\beta$ - and  $\gamma$ -CD with both various alkali metals or between their self-assemblies. Indeed, cycloligosaccharides, as cyclodextrins, are well known to be more rigid than linear or branched ones, suggesting a low probability of several stable attachment sites for the alkali cations. This prompted us to think that detection of two or more mobility peaks, especially for  $\gamma$ -CD, can be rationally ascribed to the presence of different conformers. Indeed, the distinct deducted CCS portrayed well the various size and shape of the CD based complexes, which results as a conse-

quence of a balance between size of both cationized metal (ionic radii) and CD (including eventual distortions) and more and less deep inclusion of the cation inside CD cavity (according to coordination features). Moreover, experimental data have been adequately correlated with theoretical models. In this sense, TMS can be particularly attractive to be used as a suitable molecular descriptor to enlighten parameters affecting the recognition process, to study the first sphere coordination behaviour as well as rationalization of the catalytic activities based on CD-metal supramolecular assemblies. On the other hand, TMS was also particularly efficient to highlight the presence and the identity of various orientations of the different constituent CD within hierarchical assemblies' nanotubes as well as to estimate their relative content. According to added metals, it was possible to reveal and discriminate such supramolecular edifices involving secondary/secondary hydroxyl groups (head-to head, H•H), primary/secondary rim (head-to-tail, H•T) hydroxyl groups or primary/primary rim (tail-to-tail, T•T) hydroxyl groups interactions. Such results constitute an important milestone since, at our knowledge, it is the first experimental evidences of the existence of various orientations, which until now have been only investigated by theoretical approaches. The present work paves the way for a better understanding of the topology from cyclo-oligosaccharides based supramolecular complexes, which could of course involve both other metals viz transition, post-transition rare earth or noble one, but also other cyclo-oligosaccharides based self-assemblies with or without any (bio)chemical modifications.

## **CONFLICTS OF INTEREST**

The authors declare that they have no known competing financial interests or personal relationships that could have appeared to influence the work reported in this paper.

## ACKNOWLEDGEMENTS

This work was supported by CEA and the French Ministry of Research and National Research Agency as part of the French metabolomics and fluxomics infrastructure (MetaboHUB, ANR-11-INBS- 0010 grant)

## REFERENCES

- Angelova, S. E., Nikolova, V. K., & Dudev, T. M. (2017). Determinants of the host–guest interactions between  $\alpha$ -,  $\beta$ - and  $\gamma$ -cyclodextrins and group IA, IIA and IIIA metal cations : A DFT/PCM study. *Phys. Chem. Chem. Phys.*, 19(23), 15129- 15136.
- Angelova, S., Nikolova, V., Molla, N., & Dudev, T. (2017). Factors Governing the Host–Guest Interactions between IIA/IIB Group Metal Cations and  $\alpha$ -Cyclodextrin : A DFT/CDM Study. *Inorganic Chemistry*, 56(4), 1981- 1987.
- Ao, Z., Simsek, S., Zhang, G., Venkatachalam, M., Reuhs, B. L., & Hamaker, B. R. (2007). Starch with a Slow Digestion Property Produced by Altering Its Chain Length, Branch Density, and Crystalline Structure. *Journal of Agricultural and Food Chemistry*, 55(11), 4540- 4547.
- Ben-Nissan, G., & Sharon, M. (2018). The application of ion-mobility mass spectrometry for structure/function investigation of protein complexes. *Current Opinion in Chemical Biology*, 42, 25- 33.
- Berland, K., Renaud, J. B., & Mayer, P. M. (2014). Utilizing ion mobility and tandem mass spectrometry to evaluate the structure and behaviour of multimeric cyclodextrin complexes. *Canadian Journal of Chemistry*, 93(12), 1313- 1319.

529 Bonnet, P., Jaime, C., & Morin-Allory, L. (2001).  $\alpha$ -,  $\beta$ -, and  $\gamma$ -Cyclodextrin Dimers. Molecular  
 530 Modeling Studies by Molecular Mechanics and Molecular Dynamics Simulations. *The Journal*  
 531 *of Organic Chemistry*, 66(3), 689- 692.

532 Bonnet, P., Jaime, C., & Morin-Allory, L. (2002). Structure and Thermodynamics of  $\alpha$ -,  $\beta$ -, and  $\gamma$ -  
 533 Cyclodextrin Dimers. Molecular Dynamics Studies of the Solvent Effect and Free Binding En-  
 534 ergies. *The Journal of Organic Chemistry*, 67(24), 8602- 8609.

535 Butcher, D., Chapagain, P., Leng, F., & Fernandez-Lima, F. (2018). Differentiating Parallel and  
 536 Antiparallel DNA Duplexes in the Gas Phase Using Trapped Ion Mobility Spectrometry. *The*  
 537 *Journal of Physical Chemistry B*, 122(27), 6855- 6861.

538 Charles, L., Chendo, C., & Poyer, S. (2020). Ion mobility spectrometry – Mass spectrometry cou-  
 539 pling for synthetic polymers. *Rapid Communications in Mass Spectrometry*, 34(S2), e8624.

540 Chen, Y., Zuo, Z., Dai, X., Xiao, P., Fang, X., Wang, X., Wang, W., & Ding, C.-F. (2018). Gas-  
 541 phase complexation of  $\alpha$ -/ $\beta$ -cyclodextrin with amino acids studied by ion mobility-mass spec-  
 542 trometry and molecular dynamics simulations. *Talanta*, 186, 1- 7.

543 Chouinard, C. D., Nagy, G., Webb, I. K., Garimella, S. V. B., Baker, E. S., Ibrahim, Y. M., &  
 544 Smith, R. D. (2018). Rapid Ion Mobility Separations of Bile Acid Isomers Using Cyclodextrin  
 545 Adducts and Structures for Lossless Ion Manipulations. *Analytical Chemistry*, 90(18),  
 546 11086- 11091.

547 Davis, M. E., & Brewster, M. E. (2004). Cyclodextrin-based pharmaceuticals : Past, present and  
 548 future. *Nature Reviews Drug Discovery*, 3(12), 1023- 1035.

549 Dodds, J. N., & Baker, E. S. (2019). Ion Mobility Spectrometry : Fundamental Concepts, Instru-  
 550 mentation, Applications, and the Road Ahead. *Journal of the American Society for Mass Spec-*  
 551 *trometry*, 30(11), 2185- 2195.

552 Dossmann, H., Fontaine, L., Weisgerber, T., Bonnet, V., Monflier, E., Ponchel, A., & Przybylski,  
 553 C. (2021). First Steps to Rationalize Host–Guest Interaction between  $\alpha$ -,  $\beta$ -, and  $\gamma$ -Cyclodextrin  
 554 and Divalent First-Row Transition and Post-transition Metals (Subgroups VIIB, VIIIB, and  
 555 IIB). *Inorganic Chemistry*, 60(2), 930- 943.

556 Fenn, L. S., & McLean, J. A. (2011). Structural resolution of carbohydrate positional and structural  
 557 isomers based on gas-phase ion mobility-mass spectrometry. *Physical Chemistry Chemical*  
 558 *Physics*, 13(6), 2196- 2205.

559 Frański, R., Gierczyk, B., Schroeder, G., Beck, S., Springer, A., & Linscheid, M. (2005). Mass  
 560 spectrometric decompositions of cationized  $\beta$ -cyclodextrin. *Carbohydrate Research*, 340(8),  
 561 1567- 1572.

562 French, D., Pulley, A. O., Effenberger, J. A., Rougvie, M. A., & Abdullah, M. (1965). Studies on  
 563 the Schardinger dextrans : XII. The molecular size and structure of the  $\delta$ -,  $\epsilon$ -,  $\zeta$ -, and  $\eta$ -dextrans.  
 564 *Archives of Biochemistry and Biophysics*, 111(1), 153- 160.

565 Gray, C. J., Thomas, B., Upton, R., Migas, L. G., Evers, C. E., Barran, P. E., & Flitsch, S. L.  
 566 (2016). Applications of ion mobility mass spectrometry for high throughput, high resolution  
 567 glycan analysis. *Biochimica et Biophysica Acta (BBA) - General Subjects*, 1860(8),  
 568 1688- 1709.

569 Hanozin, E., Morsa, D., & De Pauw, E. (2019). Two-Parameter Power Formalism for Structural  
 570 Screening of Ion Mobility Trends : Applied Study on Artificial Molecular Switches. *The Jour-*  
 571 *nal of Physical Chemistry A*, 123(37), 8043- 8052.

572 Haynes, W.M., Lide, J. R., Bruno, D. R. (2016). Handbook of chemistry and physics (97th ed)  
 573 Boca Raton, CRC Press.

574 Jacob, J., Geßler, K., Hoffmann, D., Sanbe, H., Koizumi, K., Smith, S. M., Takaha, T., & Saenger,  
 575 W. (1999). Band-flip and kink as novel structural motifs in  $\alpha$ -(1 $\rightarrow$ 4)-d-glucose oligosaccha-  
 576 rides. Crystal structures of cyclodeca- and cyclotetradecaamylose. *Carbohydrate Research*,  
 577 322(3), 228- 246.

578 Jeanne Dit Fouque, K., & Fernandez-Lima, F. (2019). Recent advances in biological separations  
 579 using trapped ion mobility spectrometry – mass spectrometry. *TrAC Trends in Analytical*  
 580 *Chemistry*, 116, 308- 315.

581 Jebber, K. A., Zhang, K., Cassady, C. J., & Chung-Phillips, A. (1996). Ab Initio and Experimental  
 582 Studies on the Protonation of Glucose in the Gas Phase. *Journal of the American Chemical*  
 583 *Society*, 118(43), 10515- 10524.

584 Kalenius, E., Groessl, M., & Rissanen, K. (2019). Ion mobility–mass spectrometry of supramolec-  
 585 ular complexes and assemblies. *Nature Reviews Chemistry*, 3(1), 4- 14.

586 Kfoury, M., Landy, D., & Fourmentin, S. (2018). Characterization of Cyclodextrin/Volatile Inclu-  
 587 sion Complexes : A Review. *Molecules*, 23(5).

588 Klein, C., Cologna, S. M., Kurulugama, R. T., Blank, P. S., Darland, E., Mordehai, A., Backlund,  
 589 P. S., & Yergey, A. L. (2018). Cyclodextrin and malto-dextrose collision cross sections deter-  
 590 mined in a drift tube ion mobility mass spectrometer using nitrogen bath gas. *Analyst*, 143(17),  
 591 4147- 4154.

592 Kralj, B., Šmidovnik, A., & Kobe, J. (2009). Mass spectrometric investigations of  $\alpha$ - and  $\beta$ -  
 593 cyclodextrin complexes with ortho- , meta- and para- coumaric acids by negative mode elec-  
 594 trospray ionization. *Rapid Communications in Mass Spectrometry*, 23(1), 171- 180.



595 Larriba, C., & Hogan, C. J. (2013). Ion Mobilities in Diatomic Gases : Measurement versus Pre-  
 596 diction with Non-Specular Scattering Models. *The Journal of Physical Chemistry A*, 117(19),  
 597 3887- 3901.

598 Lee, S., Wyttenbach, T., & Bowers, M. T. (1997). Gas phase structures of sodiated oligosaccha-  
 599 rides by ion mobility/ion chromatography methods. *International Journal of Mass Spectrome-*  
 600 *try and Ion Processes*, 167 - 168, 605- 614.

601 Lee, S.-S., Lee, J., Oh, J. H., Park, S., Hong, Y., Min, B. K., Lee, H. H. L., Kim, H. I., Kong, X.,  
 602 Lee, S., & Oh, H. B. (2018). Chiral differentiation of D- and L-isoleucine using permethylated  
 603  $\beta$ -cyclodextrin : Infrared multiple photon dissociation spectroscopy, ion-mobility mass spec-  
 604 trometry, and DFT calculations. *Physical Chemistry Chemical Physics*, 20(48), 30428- 30436.

605 Li, G., Delafield, D. G., & Li, L. (2020). Improved structural elucidation of peptide isomers and  
 606 their receptors using advanced ion mobility-mass spectrometry. *TrAC Trends in Analytical*  
 607 *Chemistry*, 124, 115546.

608 Liu, Y., & Clemmer, D. E. (1997). Characterizing Oligosaccharides Using Injected-Ion Mobil-  
 609 ity/Mass Spectrometry. *Analytical Chemistry*, 69(13), 2504- 2509.

610 Loftsson, T., Hreinsdóttir, D., & Másson, M. (2005). Evaluation of cyclodextrin solubilization of  
 611 drugs. *International Journal of Pharmaceutics*, 302(1), 18- 28.

612 May, J. C., Goodwin, C. R., Lareau, N. M., Leaptrot, K. L., Morris, C. B., Kurulugama, R. T.,  
 613 Mordehai, A., Klein, C., Barry, W., Darland, E., Overney, G., Imatani, K., Stafford, G. C.,  
 614 Fjeldsted, J. C., & McLean, J. A. (2014). Conformational Ordering of Biomolecules in the Gas  
 615 Phase : Nitrogen Collision Cross Sections Measured on a Prototype High Resolution Drift Tube  
 616 Ion Mobility-Mass Spectrometer. *Analytical Chemistry*, 86(4), 2107- 2116.

617 Messner, M., Kurkov, S. V., Jansook, P., & Loftsson, T. (2010). Self-assembled cyclodextrin ag-  
618 gregates and nanoparticles. *International Journal of Pharmaceutics*, 387(1), 199- 208.

619 Metzger, J. W., Jung, M., Schmalzing, D., Bayer, E., & Schurig, V. (1991). Analysis of cy-  
620 clomalto-oligosaccharides (cyclodextrins) and derivatives thereof by ion-spray mass spectrom-  
621 etry. *Carbohydrate Research*, 222, 23- 35.

622 Michelmann, K., Silveira, J. A., Ridgeway, M. E., & Park, M. A. (2015). Fundamentals of Trapped  
623 Ion Mobility Spectrometry. *Journal of the American Society for Mass Spectrometry*, 26(1),  
624 14- 24.

625 Nag, A., Chakraborty, P., Natarajan, G., Baksi, A., Mudedla, S. K., Subramanian, V., & Pradeep,  
626 T. (2018). Bent Keto Form of Curcumin, Preferential Stabilization of Enol by Piperine, and  
627 Isomers of Curcumin $\cap$ Cyclodextrin Complexes : Insights from Ion Mobility Mass Spectrome-  
628 try. *Analytical Chemistry*, 90(15), 8776- 8784.

629 Nascimento, Clebio S., Anconi, C. P. A., Dos Santos, H. F., & De Almeida, W. B. (2005). Theo-  
630 retical Study of the  $\alpha$ -Cyclodextrin Dimer. *The Journal of Physical Chemistry A*, 109(14),  
631 3209- 3219.

632 Polewski, L., Springer, A., Pagel, K., & Schalley, C. A. (2021). Gas-Phase Structural Analysis of  
633 Supramolecular Assemblies. *Accounts of Chemical Research*, 54(10), 2445- 2456.  
634 <https://doi.org/10.1021/acs.accounts.1c00080>

635 Przybylski, C., & Bonnet, V. (2013). Discrimination of cyclic and linear oligosaccharides by tan-  
636 dem mass spectrometry using collision-induced dissociation (CID), pulsed-Q-dissociation  
637 (PQD) and the higher-energy C-trap dissociation modes. *Rapid Communications in Mass Spec-*  
638 *trometry*, 27(1), 75- 87.

639 Przybylski, C., & Bonnet, V. (2021). Discrimination of isomeric trisaccharides and their relative  
 640 quantification in honeys using trapped ion mobility spectrometry. *Food Chemistry*, 341,  
 641 128182.

642 Przybylski, C., Bonnet, V., & Cézard, C. (2015). Probing the common alkali metal affinity of  
 643 native and variously methylated  $\beta$ -cyclodextrins by combining electrospray-tandem mass spec-  
 644 trometry and molecular modeling. *Phys. Chem. Chem. Phys.*, 17(29), 19288- 19305.

645 Pu, Y., Ridgeway, M. E., Glaskin, R. S., Park, M. A., Costello, C. E., & Lin, C. (2016). Separation  
 646 and Identification of Isomeric Glycans by Selected Accumulation-Trapped Ion Mobility Spec-  
 647 trometry-Electron Activated Dissociation Tandem Mass Spectrometry. *Analytical Chemistry*,  
 648 88(7), 3440- 3443.

649 Quevedo, M. A., & Zoppi, A. (2018). Current trends in molecular modeling methods applied to  
 650 the study of cyclodextrin complexes. *Journal of Inclusion Phenomena and Macrocyclic Chem-*  
 651 *istry*, 90(1), 1- 14.

652 Reale, S., Teixidò, E., & de Angelis, F. (2005). Study of Alkali Metal Cations Binding Selectivity  
 653 of  $\beta$ -Cyclodextrin by ESI-MS. *Annali di Chimica*, 95(6), 375- 381.

654 Ridgeway, M. E., Bleiholder, C., Mann, M., & Park, M. A. (2019). Trends in trapped ion mobility  
 655 – Mass spectrometry instrumentation. *TrAC Trends in Analytical Chemistry*, 116, 324- 331.

656 Ridgeway, M. E., Lubeck, M., Jordens, J., Mann, M., & Park, M. A. (2018). Trapped ion mobility  
 657 spectrometry : A short reviewMark. *International Journal of Mass Spectrometry and Ion Pro-*  
 658 *cesses*, 425, 22- 35.

659 Ruotolo, B. T., Benesch, J. L. P., Sandercock, A. M., Hyung, S.-J., & Robinson, C. V. (2008). Ion  
 660 mobility–mass spectrometry analysis of large protein complexes. *Nat. Protoc.*, 3(7),  
 661 1139- 1152.

662 Saenger, W. (1980). Cyclodextrin Inclusion Compounds in Research and Industry. *Angewandte*  
663 *Chemie International Edition in English*, 19(5), 344- 362.

664 Saenger, W., Jacob, J., Gessler, K., Steiner, T., Hoffmann, D., Sanbe, H., Koizumi, K., Smith, S.  
665 M., & Takaha, T. (1998). Structures of the Common Cyclodextrins and Their Larger Ana-  
666 logues-Beyond the Doughnut. *Chemical Reviews*, 98(5), 1787- 1802.

667 Schneider, H.-J., Hacket, F., Rüdiger, V., & Ikeda, H. (1998). NMR Studies of Cyclodextrins and  
668 Cyclodextrin Complexes. *Chemical Reviews*, 98(5), 1755- 1786.

669 Singh, M., Sharma, R., & Banerjee, U. C. (2002). Biotechnological applications of cyclodextrins.  
670 *Biotechnology Advances*, 20(5), 341- 359.

671 Song, L. X., Bai, L., Xu, X. M., He, J., & Pan, S. Z. (2009). Inclusion complexation, encapsulation  
672 interaction and inclusion number in cyclodextrin chemistry. *Coordination Chemistry Reviews*,  
673 253(9), 1276- 1284.

674 Staelens, N., Leherste, L., & Vercauteren, D. P. (2015). Formation and structural, energetic and  
675 dynamic properties of cyclodextrin host tubes and included guest molecules. *Supramolecular*  
676 *Chemistry*, 27(1- 2), 90- 109.

677 Steiner, T., & Koellner, G. (1994). Crystalline .beta.-Cyclodextrin Hydrate at Various Humidities :  
678 Fast, Continuous, and Reversible Dehydration Studied by X-ray Diffraction. *Journal of the*  
679 *American Chemical Society*, 116(12), 5122- 5128.

680 Steiner, T., & Saenger, W. (1998). Closure of the Cavity in Permethyated Cyclodextrins through  
681 Glucose Inversion, Flipping, and Kinking. *Angewandte Chemie International Edition*, 37(24),  
682 3404- 3407.

683 Suárez, D., & Díaz, N. (2017). Conformational and entropy analyses of extended molecular dy-  
684 namics simulations of  $\alpha$ -,  $\beta$ - and  $\gamma$ -cyclodextrins and of the  $\beta$ -cyclodextrin/nabumetone com-  
685 plex. *Physical Chemistry Chemical Physics*, 19(2), 1431 - 1440.

686 Sugahara, K., Horikawa, M., & Yamagaki, T. (2015). Amino-beta-cyclodextrin Complex Assisted  
687 Ionization for Labile Sesamins and their Ion-mobility Separation in ESI Q-TOF MS. *Mass*  
688 *Spectrometry Letters*, 6(1), 17- 20.

689 Szejtli, J. (1998). Introduction and General Overview of Cyclodextrin Chemistry. *Chemical Re-*  
690 *views*, 98(5), 1743- 1754.

691 Szente, L., & Szemán, J. (2013). Cyclodextrins in Analytical Chemistry : Host–Guest Type Mo-  
692 lecular Recognition. *Analytical Chemistry*, 85(17), 8024- 8030.

693 Taniguchi, H., & Honnda, Y. (2009). Amylases. In M. Schaechter (Éd.), *Encyclopedia of Micro-*  
694 *biology (Third Edition)* (p. 159- 173). Academic Press.

695 Terada, Y., Yanase, M., Takata, H., Takaha, T., & Okada, S. (1997). Cyclodextrins Are Not the  
696 Major Cyclic  $\alpha$ -1,4-Glucans Produced by the Initial Action of Cyclodextrin Glucanotransferase  
697 on Amylose. *Journal of Biological Chemistry*, 272(25), 15729- 15733.

698 Tester, R. F., Karkalas, J., & Qi, X. (2004). Starch—Composition, fine structure and architecture.  
699 *Journal of Cereal Science*, 39(2), 151- 165.

700 Wang, C., Yang, S. H., Wang, J., Kroll, P., Schug, K. A., & Armstrong, D. W. (2010). Study of  
701 complexation between cyclofructans and alkali metal cations by electrospray ionization mass  
702 spectrometry and density functional theory calculations. *International Journal of Mass Spec-*  
703 *trometry and Ion Processes*, 291(3), 118- 124.

704 Wei, J., Wu, J., Tang, Y., Ridgeway, M. E., Park, M. A., Costello, C. E., Zaia, J., & Lin, C. (2019).  
705 Characterization and Quantification of Highly Sulfated Glycosaminoglycan Isomers by Gated-

706 Trapped Ion Mobility Spectrometry Negative Electron Transfer Dissociation MS/MS. *Analyti-*  
707 *cal Chemistry*, 91(4), 2994- 3001.

708 Wenz, G. (1994). Cyclodextrins as Building Blocks for Supramolecular Structures and Functional  
709 Units. *Angewandte Chemie International Edition in English*, 33(8), 803- 822.

710 Zheng, X., Smith, R. D., & Baker, E. S. (2018). Recent advances in lipid separations and structural  
711 elucidation using mass spectrometry combined with ion mobility spectrometry, ion-molecule  
712 reactions and fragmentation approaches. *Current Opinion in Chemical Biology*, 42, 111- 118.

713